

## Electronic Supplementary Information

# The fabrication of gold nanoelectrode-nanopore nanopipette for dopamine enrichment and multimode detection

Dan Yang<sup>a</sup>, Guohui Liu<sup>a</sup>, Hongna Li<sup>a</sup>, Aoxue Liu<sup>a</sup>, Jing Guo<sup>b</sup>, Zhe Wang<sup>a\*</sup>, Yuping Shan<sup>a\*</sup> and Jin He<sup>a,b\*</sup>

<sup>a</sup> *Advanced Institute of Materials Science, Changchun University of Technology, Changchun 130012, P.R. China.*

<sup>b</sup> *Physics Department, Florida International University, Miami, 33199, United States.*

\* Corresponding author: [jh\\_ccut@outlook.com](mailto:jh_ccut@outlook.com), [wzccut@126.com](mailto:wzccut@126.com), [shanyp@ciac.ac.cn](mailto:shanyp@ciac.ac.cn);

## Contents:

S1. Fabrication of nanopore-CNE nanopipette.....	2
S2. Fabrication and characterization of nanopore-GNE nanopipette .....	3
S3. The dimension estimation of nanopore .....	5
S4. Electrochemical measurements .....	6
S5. Molecular enrichment measurements.....	7
S6. Extra data for SERS measurements.....	9
S7. References .....	13

## S1. Fabrication of nanopore-CNE nanopipette

To fabricate the nanopore-CNE nanopipette, one barrel of the dual-barrel nanopipette was sealed and butane gas was passed through the other barrel under a pressure of 30 kPa. The tip of nanopipette inserted into a quartz pipette (I.D.= 0.7mm, O.D. = 1.0 mm) under a pressure of ~0.5 kPa nitrogen gas counter-flow. Then, the tip was heated by a torch for about one min. The pyrolytic carbon quickly fills the tip and also deposited on the inner wall of the nanopipette up to the shank region (about 7 mm from the apex). The schematic fabrication of nanopore-CNE nanopipette is shown in Fig. S1a. After carbon deposition, a length of ~10 cm copper wire (0.1 mm radius) was used to contact the carbon and the connection is fixed by silver paint.

The air humidity should be below 50% in the process of CNE fabrication. The exact shape of carbon electrode at the apex depends on both the size of the nanopore opening and the pressure of butane gas. SEM result confirmed the shape of the CNE as a nanodisk electrode, as shown in Fig. S1b. The effective nanoelectrode area was estimated from the limit steady-state current ( $I_{lim}$ ) of the cyclic voltammetry. The equation is followed in below:

$$I_{lim} = 4nFDC A_{eff} \quad (S1)$$

where n is the number of electrons transferred, F is the Faraday constant (96,485 C mol<sup>-1</sup>), D is the diffusion coefficient of Ru (NH<sub>3</sub>)<sub>6</sub>Cl<sub>3</sub> (7.4×10<sup>6</sup> cm<sup>2</sup>/s), C is the bulk concentration, the A<sub>eff</sub> is the effective nanoelectrode area.

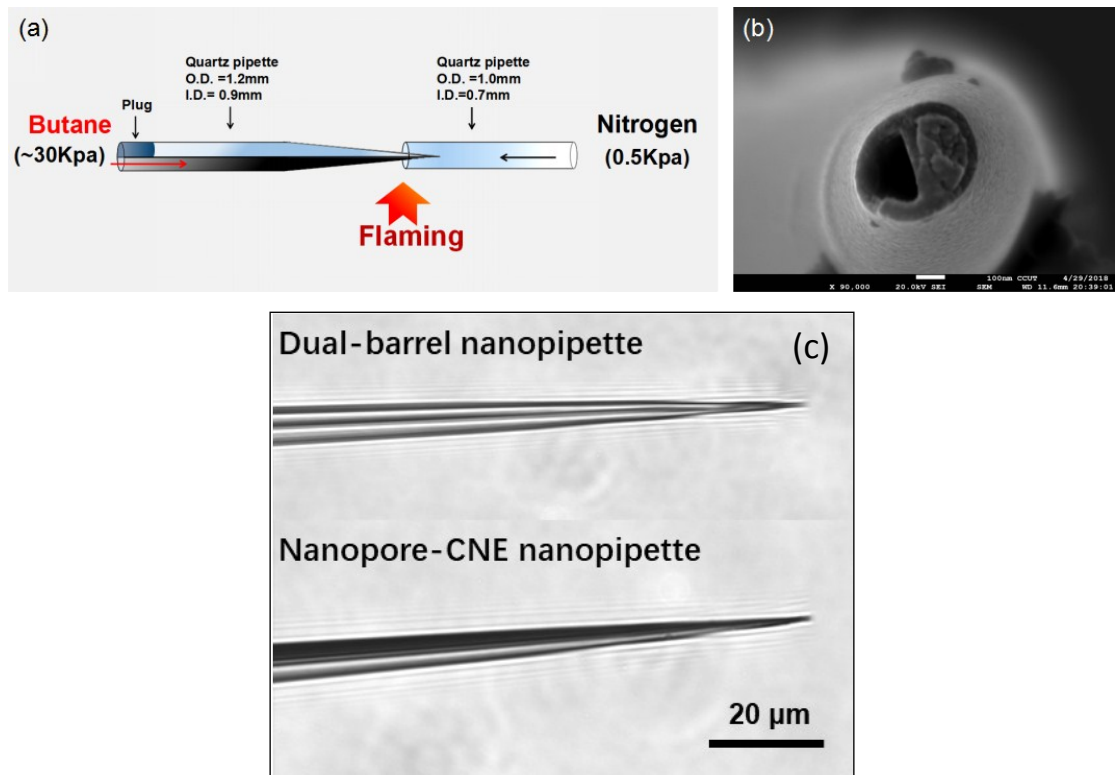


**Fig. S1.** (a) Schematic setup for the fabrication of nanopore-CNE nanopipette from the dual-nanopore nanopipette and (b) SEM image of nanopore-CNE nanopipette, scale bar is 100 nm, (c) The optical images of dual-barrel and nanopore-CNE nanopipette.

## S2. Fabrication and characterization of nanopore-GNE nanopipette

Here, we used a 10 mM  $\text{AuCl}_4^-$  containing in 1xPBS as the gold-plating solution to reduce Au (0) on the apex of CNE. A bias of -70 mV was applied on the CNE vs. an Ag/AgCl reference electrode for a few seconds. As shown in Fig. S2a, the sharp increase in the slope of the reduction current vs. deposition time curves indicates the success of deposition. The linear increase of currents (see in Fig. S2b) indicates that nanoelectrode  $A_{\text{eff}}$  is controllable. SEM in Fig. S3 characterized the different deposition times (2 s, 5 s, 10 s, 20 s, and 60 s) for nanopore-GNE nanopipettes

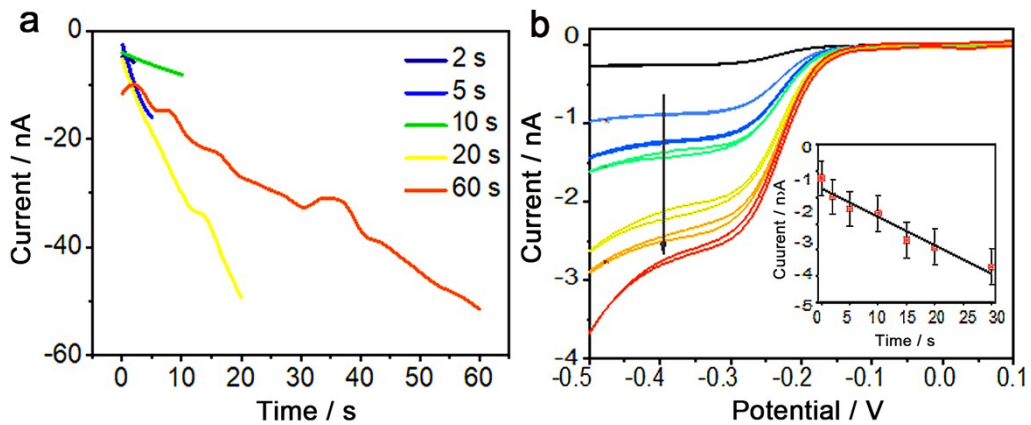


**Fig. S2.** (a) The *i-t* curves of nanopore-CNE nanopipettes applied at -70 mV bias on the CNE for different deposition times (2 s, 5 s, 10 s, 20 s, and 60 s) in the gold-plating solution; (b) The CVs of nanopore-CNE nanopipette for different deposition times (2 s, 5 s, 10 s, 15 s, 20 s and 30 s) in 1mM Ru (NH<sub>3</sub>)<sub>6</sub>Cl<sub>3</sub> containing a 1xPBS, the insert image is the linear fitting of deposition times vs. currents, the error bars are standard deviation.

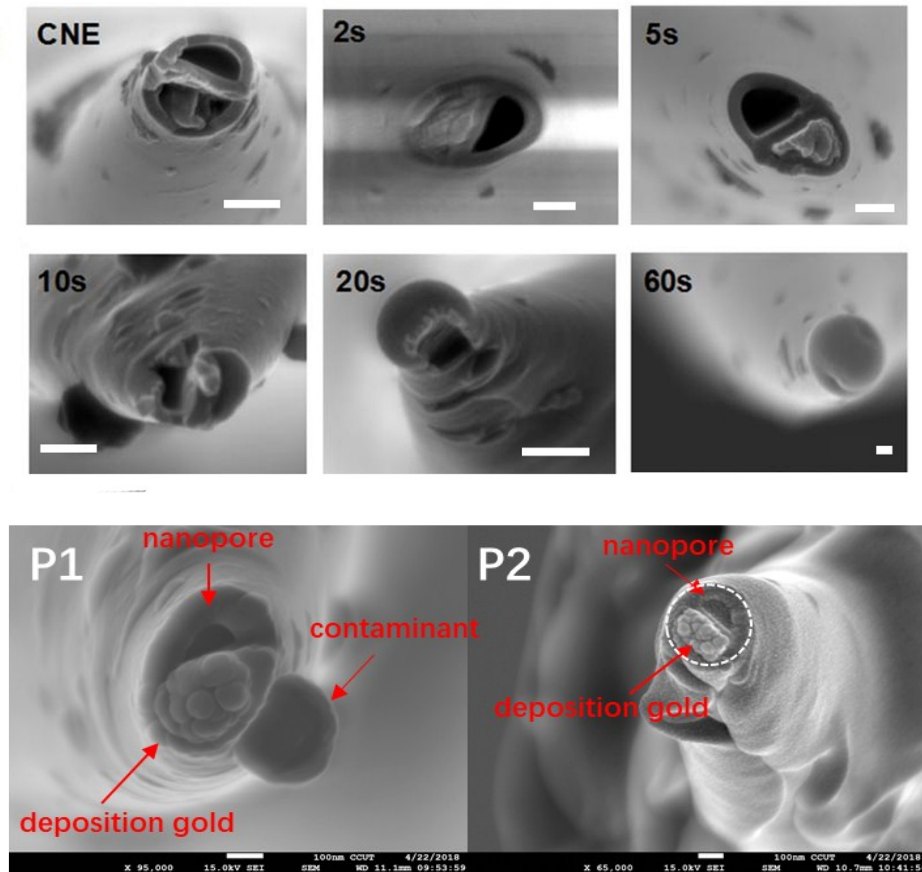


**Fig. S3.** The SEM images of nanopore-GNE nanopipettes for different deposition times (2s, 5s, 10s, 20s, and 60s), the images of P1 and P2 are the two more nanopore-GNE nanopipettes for 10s gold deposition time. All the scale bars are 100 nm.

The process of deposition for 20 nanopore-GNE nanopipettes in gold-plating solution are shown in Fig. S4a. The different initial currents depend on the different  $A_{\text{eff}}$  of the CNE. Fig. S4b shows a good repeatable potential of gold reduction (+0.68 V) for scanning five cycles in 0.5 M sulfuric acid using a GNE. Then, the nanoelectrode was stored at room temperature for the studies of stability. Compared with the currents of the 1<sup>st</sup> day and the 30<sup>th</sup> day (see in Fig. S4c), the shape of currents is almost no changed, which indicated the nanoelectrode has excellent stability.

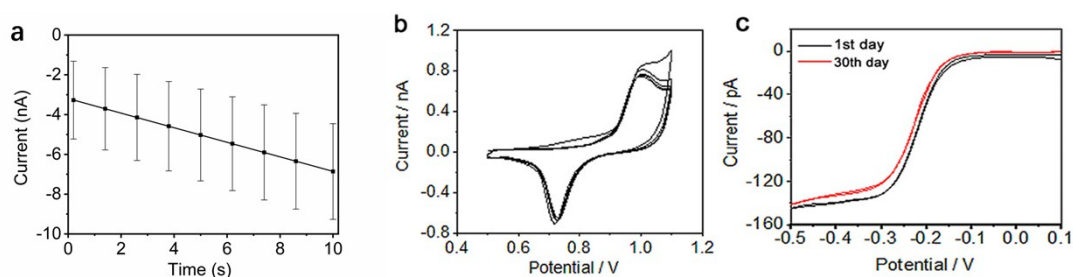


**Fig. S4.** (a) The average current change as a function of time of 20 nanopore-CNE nanopipettes in the gold-plating solution. The error is the standard deviation; (b) CVs of nanopore-GNE nanopipette scanning five cycles in 0.5 M H<sub>2</sub>SO<sub>4</sub>, scan rate is 50 mV/s; (c) CVs of the same nanopore-GNE nanopipette for 1<sup>st</sup> day and the 30<sup>th</sup> day in 1xPBS solution containing 1 mM [Ru(NH<sub>3</sub>)<sub>6</sub>]Cl<sub>3</sub>, respectively, scan rate is 50 mV/s.

### S3. The dimension estimation of nanopore

Here, as previously reported<sup>1</sup>, we used an analytical equation to estimate the inner diameter:

$$D = \frac{4}{\kappa R_p} \left( \frac{1}{\pi \tan \theta} \right) \quad (\text{S1})$$

where  $R_p$  is the resistance of nanopore, and  $\kappa$  is the conductivity of the electrolyte (10 mM PBS, pH 7.43). The  $\kappa$  (10 mM PBS) is determined to be 816.6  $\mu\text{S cm}^{-1}$ . When using  $\theta = 5^\circ$  as an average half cone-angle, the estimated inner diameter of

nanopore is about  $110 \pm 28.68$  nm, which is consistent with the results of SEM. Fig. S5 shows the ionic current through the nanopores of 20 dual-nanopore nanopipettes, nanopore-CNE nanopipettes, and nanopore-GNE nanopipette, respectively. Nanopores were applied at the range from -400 mV to +400 mV in 10 mM PBS. The mean values of  $R_p$ , inner diameter and rectification ratio for dual-nanopore, nanopore-CNE, and nanopore-GNE nanopipette are shown in Table S1, respectively.

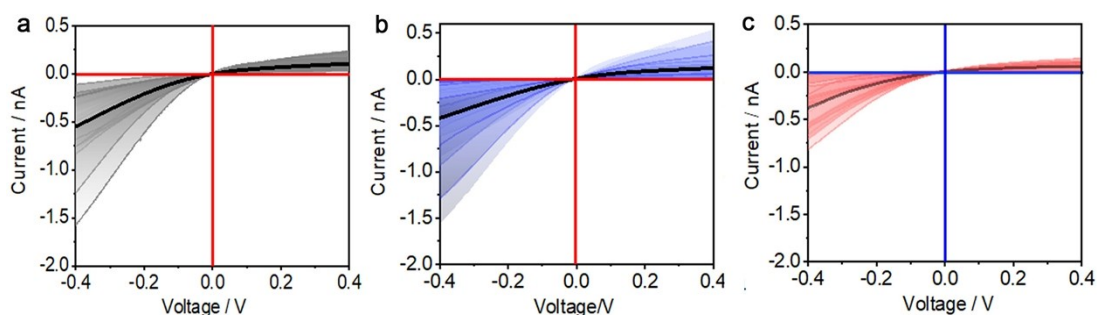


**Fig. S5.** The 20 I-V curves of (a) dual-nanopipettes (gray plots), (b) nanopore-CNE nanopipettes (blue plots) and (c) nanopore-GNE nanopipettes (red plots), respectively.

**Table S1.** The mean values of  $R_p$ , diameter, and rectification ratio of dual-nanopore, nanopore-CNE, and nanopore-GNE nanopipette, respectively.

Designation	Dual-barrel nanopipette	Nanopore-CNE nanopipette	Nanopore-GNE nanopipette
$R_p$ ( $G\Omega$ )	$1.70 \pm 0.7$	$1.71 \pm 1.00$	$2.68 \pm 0.58$
Diameter (nm)	$81 \pm 28.68$	$77 \pm 17.50$	$56 \pm 11$
Rectification ratio (r)	$0.20 \pm 0.05$	$0.28 \pm 0.04$	$0.15 \pm 0.05$

#### S4. Electrochemical measurements

Fig. S6a shows two imperfect sigmoid-shaped voltammograms at around the potential of +200 mV for nanopore-CNE and nanopore-GNE nanopipette, respectively. Although two nanoelectrodes have higher capacitive background currents in a high concentration of DA (100  $\mu$ M), the GNE exhibits a higher

electrochemical response than CNE.

Likewise, the nanopore-CNE nanopipette was also measured on DPVs with successive addition of different concentrations of DA in 10 mM PBS solution. In the Fig. S6b, the increase in currents shows a similar trend with the GNE; however, the responses are weaker than GNE. Two linear ranges from 0 to 150 nM and 150 to 600 nM, as shown in Fig. S6c, corresponding the linear equations are fitting as  $I_1 = 0.048C_{\text{DA}} + 1.416$  ( $R_1^2 = 0.999$ ) and  $I_2 = 0.017C_{\text{DA}} + 5.046$  ( $R_2^2 = 0.965$ ), respectively. The sensitivities are  $0.048 \text{ pA nM}^{-1}$  and  $0.017 \text{ pA nM}^{-1}$ , respectively. The lower slope above 150 nM is due to the supersaturation of DA on the surface of CNE.

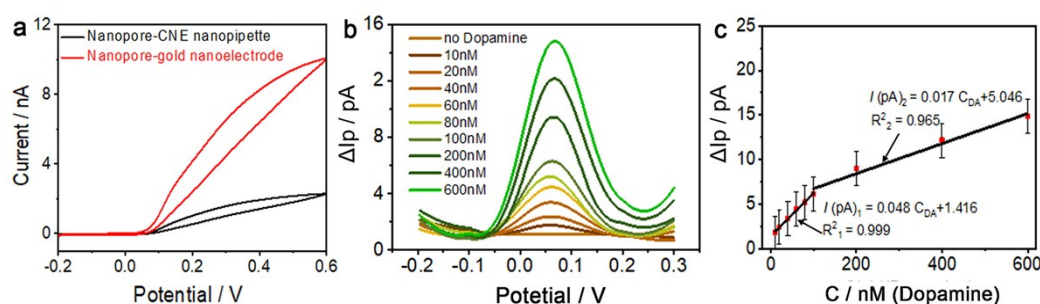


**Fig. S6.** (a) The CVs of nanopore-CNE and nanopore-GNE nanopipette in 100  $\mu\text{M}$  DA containing 10 mM PBS solution, scan rate is 50 mV/s, respectively; (b) DPVs of nanopore-CNE nanopipette for different concentrations DA (0 nM, 10 nM, 20 nM, 40 nM, 60 nM, 80 nM, 100 nM, 200 nM, 400 nM and 600 nM); (c) The linear fits of the currents vs. DA concentrations, the error bars represent standard deviations.

## S5. Molecular enrichment measurements

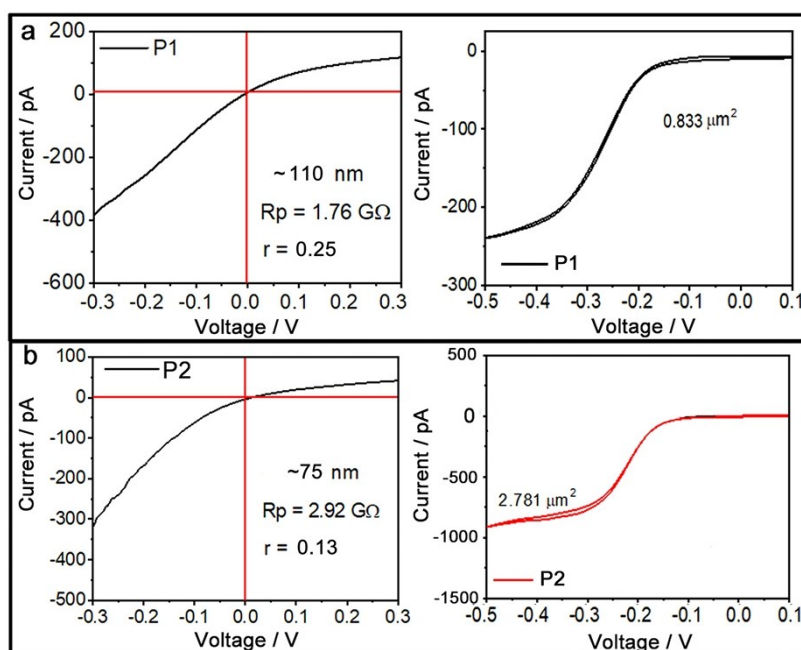
We used a nanopore-CNE nanopipette (P1,  $\sim 85 \text{ nm}$ ,  $0.833 \mu\text{m}^2$ ) and a nanopore-GNE nanopipette (P2,  $\sim 53 \text{ nm}$ ,  $2.781 \mu\text{m}^2$ ) (see in Fig. S7a and S7b) for the comparison of the enrichment effect, respectively. P1 was measured with the DC enrichment in 100 nM DA solution. The results of P1 enrichment, as shown in Fig. S8a and S8b, the CNE is less effective than GNE.

Fig. S9a and S9b show the influence of pH on DA enrichment. In neutral solutions,

the enrichment effect is not obvious. When the pH of buffer reaches up to 8, the enrichment effect becomes worse and eventually forms polydopamine.

100 nM AA was measured on the nanopore-GNE nanopipette under the same enrichment conditions. The DPV results are shown in Fig. S9c, The DPV results are shown in Fig. S9c, where AA acts as a negatively charged molecule that can be repelled by electric field force, making the nanopore selective to  $DA^+$ .

The stability of the DA molecule at high negative potential during enrichment was verified by scanning from +900 to -600 mV measured on CV in 10 mM DA solution (see Fig. S9d).



**Fig. S7.** (a) The I-V and CV curves of a nanopore-CNE nanopipette (P1) and a nanopore-GNE nanopipette (P2), respectively.

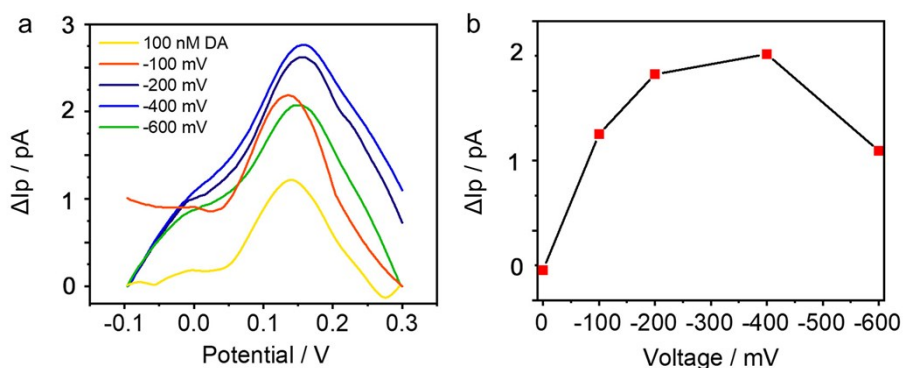


**Fig. S8.** The DPVs of 100 nM DA for nanopore enrichment at the different bias (-100 mV, -200 mV, -400 mV and -600 mV) on the nanopore using P1, and (b) the corresponding the plot of the relationship between bias and current.

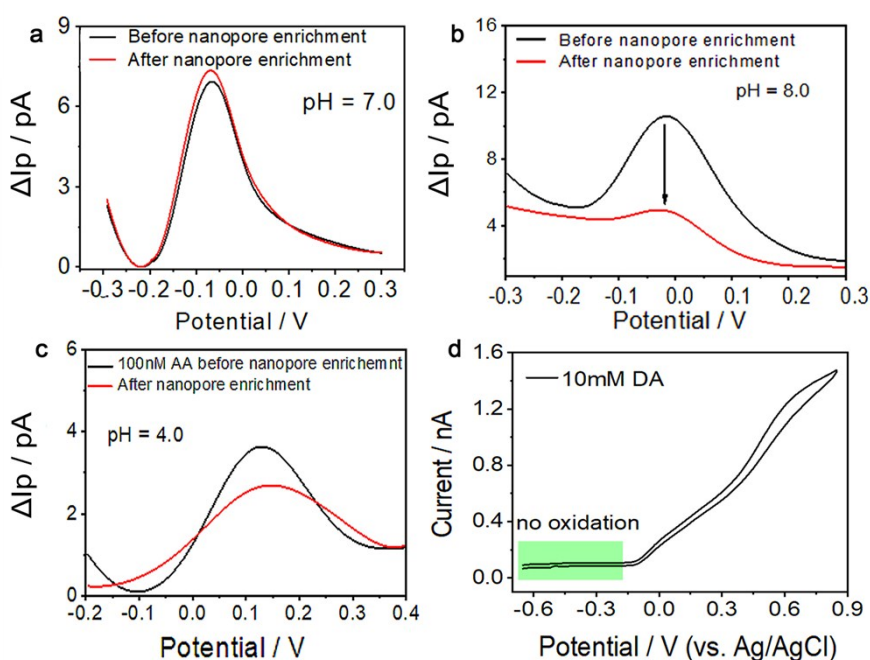


**Fig. S9.** (a, b) DPVs of before and after nanopore enrichment for 100 nM DA in the pHs (7.0 and 8.0) of 10 mM citric acid- $\text{Na}_2\text{HPO}_4$  buffers, respectively; (c) DPVs of before and after nanopore enrichment for 100 nM AA in a 10 mM citric acid- $\text{Na}_2\text{HPO}_4$  buffer (pH 4.0), respectively; (d) CV of 10 mM DA in the citric acid- $\text{Na}_2\text{HPO}_4$  buffer (pH 4.0) with the scanning range from -600 to +900 mV, scan rate is 50 mV/s.

## S6. Extra data for SERS measurements

The results of DLS and zeta potential are shown in Fig. S10a and S10b, indicating that the synthesized AgNPs are negatively charged (-19.09 mV) in aqueous solution and have a diameter of  $\sim 54$  nm. The UV-vis absorption peaks of AgNPs were observed at 440 nm. After adding  $\sim 7$  pM AgNPs into a 100 nM DA solution, an

absorption peak was recorded every 30s (see in Fig. S10c). The decreased absorption peaks intensity demonstrates DA<sup>+</sup> molecules can rapidly bind to the AgNPs within 5 mins. Due to the bonding of the catechol group of DA and AgNPs, zeta potential becomes change to +4.82 mV, which also results in aggregation and poor electrochemical responses (Fig. S10f).

The Raman characteristic peak of the dopamine powder is shown in Fig. S10d. The experimentally measured the Raman characteristic peaks of dopamine with their tentative assignments are shown in Table S2. From the Fig. S10e, after nanopore enrichment, the SERS signals of DA were not enhanced for the nanopore-CNE nanopipette. Instead, we obtained a representative Raman signal of crystalline carbon, which is derived from the carbon at the apex of CNE. Therefore, it can be indicated that the deposition gold serves as a SERS-enhanced substrate is contributed to improve the analyte Raman signals.

Fig. S11 shows the Raman results of before and after nanopore enrichment and AC DEP enrichment in the 100 nM DA when not the addition of AgNPs. Both nanopore enrichment and AC DEP enrichment are not shown the enhanced the Raman signals

Similar Raman results have been acquired from 10 nanopipettes. We also examined the reproducibility of DA detection by repeating experiments on the same nanopipette. After finishing one experiment, the nanopipette was rinsed by DI water and repeated all the measurements, including enrichment and SERS measurements. We repeated three times and the SERS results are shown in Fig. S12.

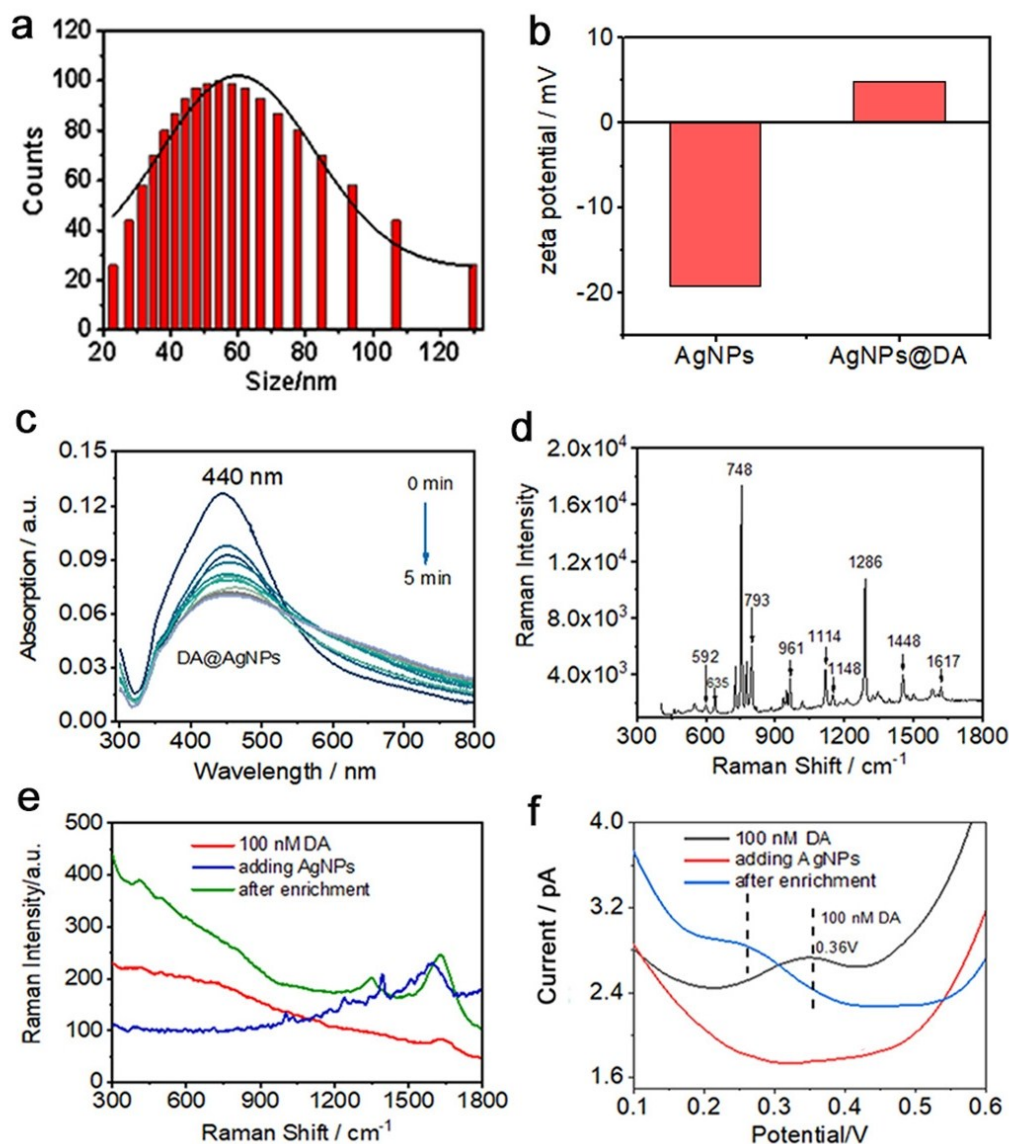


**Fig. S10.** (a) The size distribution of synthetic AgNPs and (b) the zeta potentials of AgNPs and DA@AgNPs in an aqueous solution; (c) UV-vis absorption spectra of  $\sim 7$  pM AgNPs was added into the 100 nM DA solution, respectively; (d) Raman spectrum of the powder DA; (e) Raman spectra of nanopore-CNE nanopipette for 100 nM DA with adding 7 pM AgNPs, then nanopore enrichment for 5 mins; (f) DPVs of 100 nM DA, after adding 7 pM AgNPs, then nanopore enrichment for 5 mins.

**Table S2.** Experimentally measured Raman vibrations of dopamine with their tentative assignments.

Powder Measured ( $\text{cm}^{-1}$ )	Measured ( $\text{cm}^{-1}$ )	Assignment <sup>2</sup>
	412	ring deformation + CH,
635	634	aromatic $\nu$ CC + $\omega$ CH
	714	ring deformation + $\gamma$ CH
748		ring deformation + $\gamma$ CH
793		
961		ring deformation + $\tau$ NH + $\omega$ CH
	1005	

1029	1034	$\omega$ CH
1060	1059	$\nu$ C-C-N + $\omega$ CH
1114	1113	$\omega$ CH + $\tau$ NH + $\nu$ CN
1148		
	1169	weak ring breathing + aromatic $\rho$ CH
1286	1279	ring breathing + aromatic $\rho$ CH + $\tau$ CH
1387	1398	$\omega$ CH + $\tau$ NH
1466	1465	$\delta$ CH
	1505	$\nu$ CC + $\delta$ CH
	1583	
1615	1610	ring deformation + $\delta$ OH

[a] cited from ref. 2

[b] the notations of the modes are wagging ( $\omega$ ); out-of-plane bending ( $\gamma$ ); twisting ( $\tau$ ); stretching ( $\nu$ ); rocking ( $\rho$ ); scissoring ( $\delta$ ), respectively.

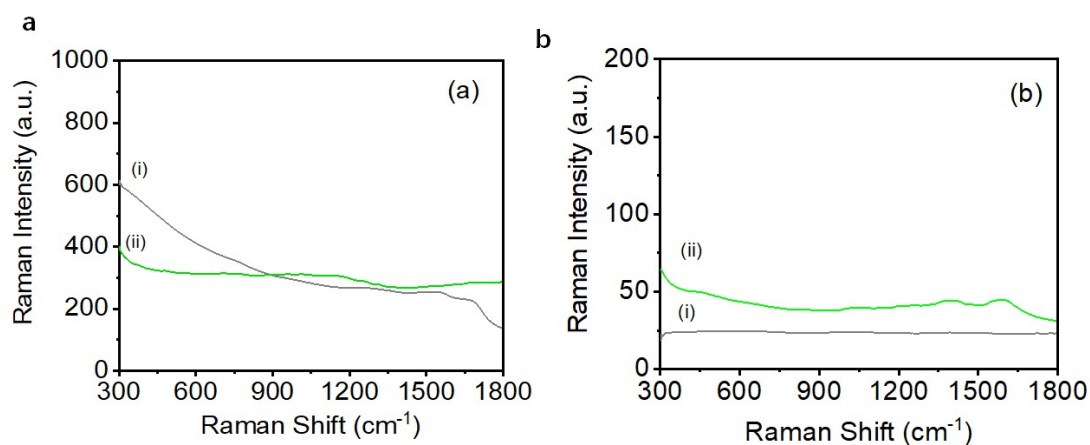


**Fig. S11.** (a) The SERS spectra before (i, black color) and after (ii, green color) 5-min nanopore enrichment. (b) The Raman spectra before (i, black color) and after (ii, green color) 1 min AC DEP enrichment. For both cases, there is 100 nM DA in the solution but no AgNPs are added.

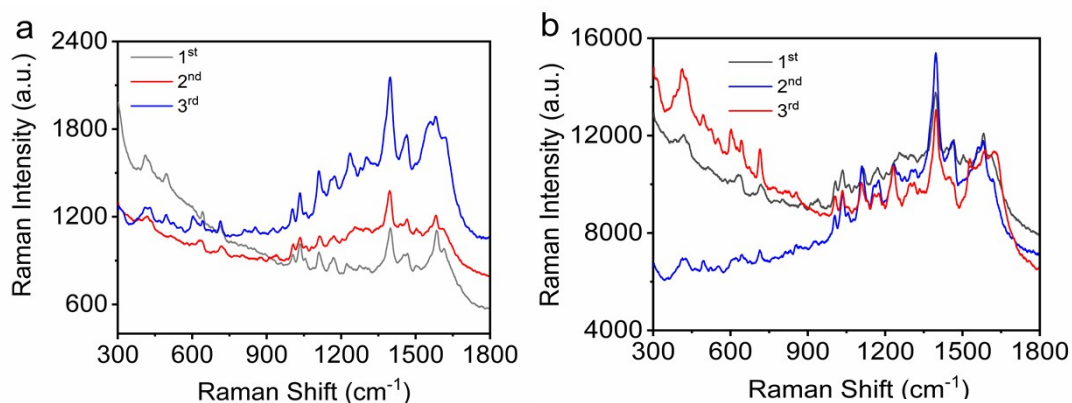


**Fig. S12.** The Raman spectra after repeated the (a) the nanopore and (b) AC DEP enrichment three times in 100 nM DA solution with 7 pM AgNPs.

## S7. References

1. Panday, N.; Qian, G.; Wang, X.; Chang, S.; Pandey, P.; He, J., Simultaneous Ionic Current and Potential Detection of Nanoparticles by a Multifunctional Nanopipette. *ACS Nano* **2016**, *10* (12), 11237-11248.
2. Shereema, R., Electrochemical Detection of Dopamine in Presence of Serotonin and Ascorbic acid at Tetraoctyl ammonium bromide Modified Carbon Paste Electrode: A Voltammetric Study. *Journal of Biosensors & Bioelectronics* **2015**, *06* (02).